

Interpretation of the photoelectron spectra of superalkali species: Li_3O and Li_3O^-

Cite as: J. Chem. Phys. **135**, 164307 (2011); <https://doi.org/10.1063/1.3636082>

Submitted: 30 June 2011 . Accepted: 19 August 2011 . Published Online: 27 October 2011

S. Zein, and J. V. Ortiz



View Online



Export Citation

ARTICLES YOU MAY BE INTERESTED IN

[Thermochemical properties of gaseous \$\text{Li}_3\text{O}\$ and \$\text{Li}_2\text{O}_2\$](#)

The Journal of Chemical Physics **70**, 1815 (1979); <https://doi.org/10.1063/1.437656>

[Interpretation of the photoelectron spectra of superalkali species: \$\text{Na}_3\text{O}\$ and \$\text{Na}_3\text{O}^-\$](#)

The Journal of Chemical Physics **136**, 224305 (2012); <https://doi.org/10.1063/1.4728073>

[Photoelectron spectroscopy of the molecular anions, \$\text{Li}_3\text{O}^-\$ and \$\text{Na}_3\text{O}^-\$](#)

The Journal of Chemical Physics **135**, 164308 (2011); <https://doi.org/10.1063/1.3657854>

Lock-in Amplifiers
up to 600 MHz



Interpretation of the photoelectron spectra of superalkali species: Li_3O and Li_3O^- a)

S. Zein and J. V. Ortiz^{b)}

Department of Chemistry and Biochemistry, Auburn University, Auburn, Alabama 36849-5312, USA

(Received 30 June 2011; accepted 19 August 2011; published online 27 October 2011)

The present paper deals with the interpretation of the photoelectron spectrum of the Li_3O^- . After several failed attempts to attribute all of the observed peaks in the experimental spectrum to anionic species, neutral species were considered assuming a sequential two-photon absorption mechanism. We find that only two of the six observed peaks can be attributed to photodetachments and that all other observed features can be assigned to ionizations from the ground and excited states of the neutral. Nuclear distributions other than three lithium atoms surrounding the oxygen are not likely to be stable. The interpretation of the experimental peak located at about 1.2 eV remains challenging. It can either be attributed to the second electron detachment (involving the HOMO -1 orbital) energy from the anion's triplet C_{2v} state or to higher excited states (involving HOMO $+10$, 11 , 12 , ... orbitals) of the neutral species. Furthermore, we have examined the influence of vibrational displacements on the location of the observed peaks. We find that this effect is smaller than 0.05 eV and, therefore, must be considered as negligible. © 2011 American Institute of Physics. [doi:10.1063/1.3636082]

INTRODUCTION

Superatoms are molecular species that sometimes resemble atoms of the alkali or halogen families.¹ Superalkalies constitute valuable molecules with strong electropositive (electron donation) character that can be used in diverse applications as, for instance, building blocks of novel ionic solids.² Superalkalies are characterized by highest occupied molecular orbitals (HOMO) with a non-bonding or antibonding character that favors an electron detachment at lower energies. Among the most prominent superalkalies is the trilithium oxide molecule that is attracting much attention from the experimental and theoretical standpoints.³⁻⁹ Li_3O is a stable molecule in a bound state that breaks the octet rule by having one excess electron.¹⁰⁻¹² The anion species of the same molecule possesses a relatively low electron detachment energy of about 0.65 eV.³

Several computational and experimental studies were dedicated to hyperlithiated molecules³⁻⁶ starting with Kudo's works in 1978.⁶ The first ionization energy of the Li_3O molecule was first found experimentally to be 4.54 ± 0.2 eV,⁷ a number that was later corrected from *ab initio* calculations or more recently joint experimental and computational chemistry studies to be 3.59 ± 0.02 eV.^{3,4} Gutowski and Simons³ discussed in detail the neutral and anionic species that turned out to be rich in stable minima. Four (one D_{3h} and three C_{2v}) bound ground states, studied at the coupled cluster singles and doubles plus perturbative triples or CCSD(T) (Refs. 13 and 14) level of theory for geometry optimizations and complete active space plus second-order perturbation theory or CASPT2 for excited electronic states energies, were found for the neutral species. As for the anionic species, a

D_{3h} singlet ground state was predicted with 0.66 eV as the VEDE (vertical electron detachment energy) followed by a C_{2v} triplet excited state (lying 0.21 eV higher). The latter state was predicted to have its first two VEDEs at 0.45 and 1.15 eV. Unfortunately, the above-mentioned studies considered only the ground and the first few excited states that are less than 2.0 eV above the ground state, probably because the experimental techniques available at that time were more limited than those of current spectrometers.

Recently the photoelectron spectrum of the Li_3O^- was reported, in the Bowen group,¹⁵ at a laser energy range up to 3.5 eV. Several peaks were observed at the experimental temperature, including the previously predicted peaks (around 0.5 and 1.2 eV) assigned to the lowest singlet and triplet states of the anion. Following these peaks there exist other close ones that are more challenging for interpretation. This raises several questions that we will try to answer in the present paper: (i) Do the peaks between 1.5 and 3.5 eV correspond to the anion or do they arise from the ionization of Li_3O ? (ii) Is the peak at 1.1 eV indicative of the presence of anionic species or could it be associated with higher excited states of neutral species? (iii) Are there atomic distributions other than three lithium atoms surrounding an oxygen atom that can exist as a bound state? (iv) Can vibronic effects be seen in the reported spectra? After a brief description of theoretical methods and computational strategies, two other sections will follow describing the molecular geometries and the electronic structures of trilithium oxide. The main results will be reviewed in the summary and conclusions section at the end of the paper.

DYSON ORBITALS

In electron propagator theory (EPT), the Dyson equation provides the foundation of practical calculations and

^{a)}This paper is presented in honor of the 60th birthday of Professor A. I. Boldyrev of Utah State University.

^{b)}Electronic mail: ortiz@auburn.edu.

subsequent, qualitative interpretation. All of the solutions of the Dyson equation may be cast in the following form:

$$[\mathbf{F} + \Sigma(\varepsilon_i)] \Phi_i = \varepsilon_i \Phi_i, \quad (1)$$

where \mathbf{F} and Σ are the Fock and self-energy operator matrices, respectively. Φ is a Dyson orbital (DO) that is defined as the overlap between the N and $N-1$ many-electron wave functions according to,

$$\Phi(1) = \sqrt{N} \int \Psi_I^N(1, \dots, N) \Psi_F^{N-1}(2, \dots, N) d2, \dots, dN. \quad (2)$$

I and F stand for initial and final states. Φ can be built from the canonical Hartree-Fock molecular orbitals, as in the cases of the outer valence Green's function method (OVGF) (Ref. 16 and partial third-order approximation (P3) (Ref. 17) methods, or from Brueckner orbitals^{18,19} as in the Brueckner doubles plus triple field operator or BD-T1 case.²⁰⁻²² Dyson orbitals are also necessary for calculations of Compton profiles,²³ electron momentum spectra,^{24,25} and interpretation of other orbital imaging experiments.²⁶⁻²⁸

In general, the DOs are not normalized to unity. Their norms represent the pole strengths (PS) and may vary between 0 and 1, such that

$$\text{PS} = \int |\Phi(1)|^2 d1. \quad (3)$$

Photoionization intensities, transition probabilities, and electron scattering cross sections are proportional to the pole strengths. Another comprehensible definition of the PS can be seen, according to the quasiparticle approach,²⁹ in the following expression:

$$\text{PS} = \frac{1}{1 - \left. \frac{d\Sigma(E)}{dE} \right|_{E=\varepsilon}}, \quad (4)$$

where the dependence of the PS on the variation of the self-energy becomes obvious.

NORMAL MODE DISPLACEMENTS

Nuclear motion is much slower than electronic redistribution in photoionization experiments.³⁰ The time scale for nuclear motion is on the order of picoseconds whereas electronic phenomena take place in the femtosecond range.³⁰ Vibrational displacements along normal modes were considered previously for the interpretation of the electronic spectra of Li_3O .⁵ Band broadenings due to vibrational motions were found to be as much as 0.3 eV. A recent study considered the lowest three normal modes arguing that at about 200 K, the assumed temperature of the experiment, only these modes can be populated.⁵ If the zero-point population of each normal mode is included, all six normal modes should be considered because thermal population is here not taken yet into account by definition. One-dimensional treatment of the problem might also be risky since the normal mode displacements are multidimensional as is shown in Fig. 1.

We advocate a simple consideration of the harmonic approximation. *A priori* this is a safe starting point, we do not

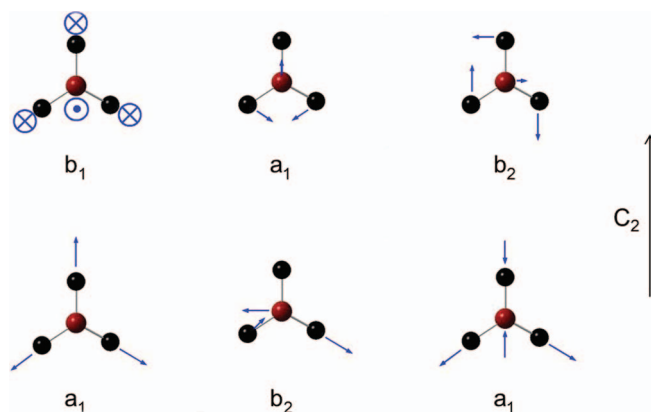


FIG. 1. Normal modes of the triplet ground state (C_{2v} symmetry).

expect major changes in the nuclear positions at the ZPE (zero-point energy) of each mode. Given the normal displacement matrices, \mathbf{Q} , from a quantum chemical calculation, typically a numerical frequency analysis using the CCSD(T) method, we can start by calculating the total electronic energy at a probe geometry obtained, for example, by moving the atoms by a small fraction (a_1) along normal mode. Thus, if \mathbf{X}_0 is the matrix of the Cartesian coordinates at the minimum on the potential energy surface and \mathbf{Q} is the displacement matrix, then the probe geometry \mathbf{X}_1 is defined by,

$$\mathbf{X}_1 = \mathbf{X}_0 + a_1 \mathbf{Q}. \quad (5)$$

Having obtained the relative energy of the \mathbf{X}_1 geometry ($E_1 - E_0$) from a single point calculation we can determine the fraction of the normal mode a_2 at the far-side turning point of the considered mode. At the far-side turning point, the total energy is the ZPE, and

$$a_2 = a_1 \sqrt{\frac{E_{\text{ZPE}}}{E_1 - E_0}}. \quad (6)$$

One can easily check that the new geometry defined as

$$\mathbf{X}_2 = \mathbf{X}_0 + a_2 \mathbf{Q} \quad (7)$$

possesses the ZPE as $E_2 - E_0$ by performing a single point energy calculation. When this condition is not satisfied, this would indicate that the geometry is too far from the minimum (i.e., a_1 is too big) and the harmonic approximation is now invalid. One can simply overcome this problem by reiterating the formula starting from the \mathbf{X}_2 geometry. Here, the new geometry must be closer to the minimum and typically convergence can be achieved within three iterations.

COMPUTATIONAL DETAILS

All calculations were carried out using the GAUSSIAN 03 (Ref.31) package. The 6-311+G* /CCSD(T) (Refs. 32 and 33) level of theory was used for geometry optimizations and numerical (double differentiation) frequency analysis as well as for the single point calculations of several electronic states at each minimum for the estimation of vertical transition energies.

Several computational methods of the EPT³⁴ were used for the direct estimation of the VEDEs in combination with several basis sets. OVGf,¹⁶ P3,¹⁷ and a method based on Brueckner-doubles (BD) (Refs. 18 and 19) orbitals, i.e., BD-T1.^{20,21} BD-T1 is used for closed shell initial states, and OVGf and P3 were reserved for the open-shell initial states. Whereas the first and second VEDEs of the anionic species were calculated directly, we used another approach for the estimation of the ionization potentials of the excited states of the neutral. Electron affinities of the cationic species correspond to ionization potentials of the neutral. It will be shown later that this approach is useful for the interpretation of the experimental spectra. Ten basis sets were tested for the estimation of the VEDE from two EPT methods (see supplementary material Ref. 35). Each of the predefined 6-311+G*, 6-311+G(2df), and 6-311+G(3d2f) sets (basis sets 1, 4, and 7, respectively) was supplemented by one or two diffuse sets of s and p functions defined by dividing the smallest (Gaussian function) exponents of the Li and O atoms by 3 and 9. The first additional set is included in basis #2 and both sets are included in basis #3. A similar argument applies to the generation of sets 5 and 6 from basis 4 and to the generation of sets 8 and 9 from basis 7. For comparison, aug-cc-pvtz (#10) (Ref. 36) results are compared to those from Pople basis sets.

Results and discussions

Molecular geometries

Geometry optimizations were first performed using the coupled-cluster single and double (CCSD) (Ref. 37) method starting from C_{3v}, D_{3h}, and C_{2v} geometries in an attempt to have a large scan of the potential energy surface. Two starting points were further considered for the C_{2v} point group: two long with one short (2L) and two short with one long (1L) Li–O distances. At the CCSD level, D_{3h} and C_{2v} (1L) were found to be unique ground states for the singlet and triplet states of the Li₃O⁻ species, respectively. C_{2v} (2L) was found to be a stationary point for the neutral Li₃O species. Single-point CCSD(T) calculations of the VEDEs at the D_{3h} and C_{2v} (2L) geometries were also performed. The energy of the doublet at the (singlet) D_{3h} geometry was found to be lower. However, frequency analysis showed that the C_{2v} (2L) structure is a stationary point at the CCSD level of theory. This was a sign that the CCSD and CCSD(T) potential energy surfaces may disagree about the correct minimum structure.^{3–5} For this reason, we had to check the CCSD results by performing more costly numerical CCSD(T) geometry optimizations and vibrational analysis starting from different points of the potential energy surface of each electronic state.

Twelve geometry optimizations were performed starting from four structures and three electronic states. C_{3v} (dihedral angle = 112°) and the two C_{2v} geometries obtained from CCSD calculations together with the optimized D_{3h} structures were considered for geometry optimizations of the singlet, triplet (anionic), and doublet (neutral) states. Only three minima were obtained. D_{3h} with d_{Li–O} = 1.702 and 1.699 Å were found for the singlet and doublet states, respectively. The triplet state has C_{2v} (1L) symmetry with d_{Li–O} = 1.725

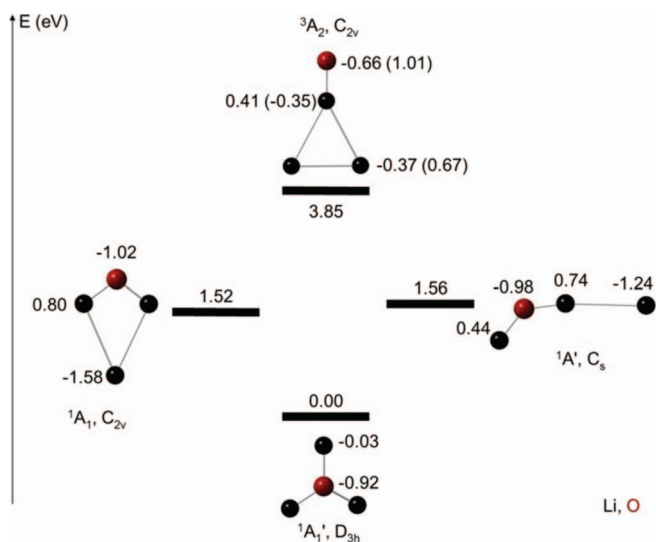


FIG. 2. Energy levels of several Li₃O⁻ structures with different nucleus distributions relative to the D_{3h} structure. Mulliken charge distributions are provided next to each atom. In the case of a triplet ground state (top), the spin density population is indicated in parentheses.

and 1.703 Å and Li–O–Li = 128.2°. Similar problems arising from the inclusion of perturbative triple excitation corrections were encountered previously in the calculations on the doublet state.^{3,38}

Further structural inspections have been performed starting from nuclear distributions other than a central oxygen surrounded by the three lithium atoms (see Fig. 2). It turns out that the new minima are over 1.5 eV higher than the ground D_{3h} state at the CCSD(T) level of theory. These geometries will not be considered further for the interpretation of the experimental photoelectron spectra treated in this paper. They are very unlikely to be thermally populated under experimental conditions, for 1 eV corresponds to about 11 600 K.

Electronic states

As understood from the Molecular geometries section, states labeled by the totally symmetric irreducible representation were obtained for the singlet, doublet, and triplet, ¹A₁', ²A₁', and ³A₁, respectively. The ¹A₁' state lies 0.217 eV under the ³A₁ state and 0.645 eV under the ²A₁' state (Table I and Fig. 3). In the harmonic approximation, these two values become 0.218 and 0.642 eV, respectively, because of the ZPE corrections. VEDEs were estimated to be 0.447 and 0.646 eV from the triplet and singlet states, respectively, to the doublet. These values are summarized in the following tables and will

TABLE I. Adiabatic and vertical transition energies between electronic states of Li₃O⁻ and Li₃O from 6-311+G*/CCSD(T). ¹A₁' and ³A₁ are anions, ²A₁' is neutral.

	Adiabatic (eV)	Adiabatic with ZPE	Vertical
¹ A ₁ ' → ² A ₁ '	0.65	0.64	0.65
³ A ₁ → ² A ₁ '	0.43	0.42	0.45

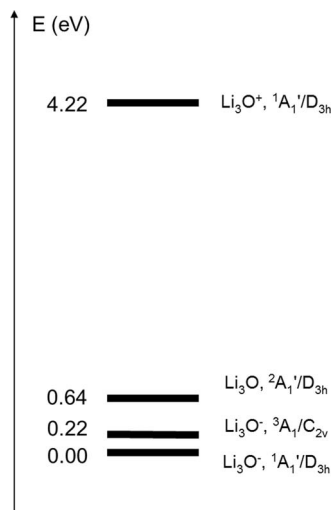


FIG. 3. Relative energies of various charge and electronic states calculated at the 6-311+G*/CCSD(T) level and including zero-point energies.

help us as references for assessing the quality of the electron propagator approximations.

Analysis of the electronic and spin density distributions allows more insight into the detachment and molecular relaxation processes (Fig. 4). Indeed, the singlet state (left bottom) has a zero spin density everywhere until an electron is detached that opens the shell with one unpaired electron. This doublet state at the geometry of the singlet (top left) possesses more important spin polarizations on the Li atoms than on the oxygen. One can notice here that the charge and spin density distributions do not change when the molecular structure relaxes (to center) to the doublet electronic state's minimum. This is expected because the structural changes are still minor in this case, unlike the relaxation from C_{2v} to D_{3h} . The

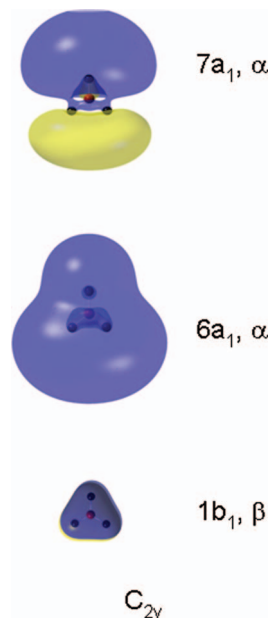


FIG. 5. Highest occupied molecular orbitals with spin up (α) and down (β) of the triplet ground state (isovalue = 0.005).

triplet ground state (bottom right) concentrates the unpaired electrons mainly on the Li atoms. Almost one unpaired electron is localized on the Li atom on the z axis (longer Li–O distance) and the second spin is shared by the two other equivalent Li atoms. This can be understood from the shape of the molecular orbitals (MO) given in Fig. 5.

The two unpaired electrons occupy α spin-orbitals $6a_1$ and $7a_1$. $1b_1 \beta$ has a shape similar to $1b_1 \alpha$. These two latter spin-orbitals have similar shapes similar to that of the $1a_2''$ HOMO–1 of the singlet (Fig. 6).

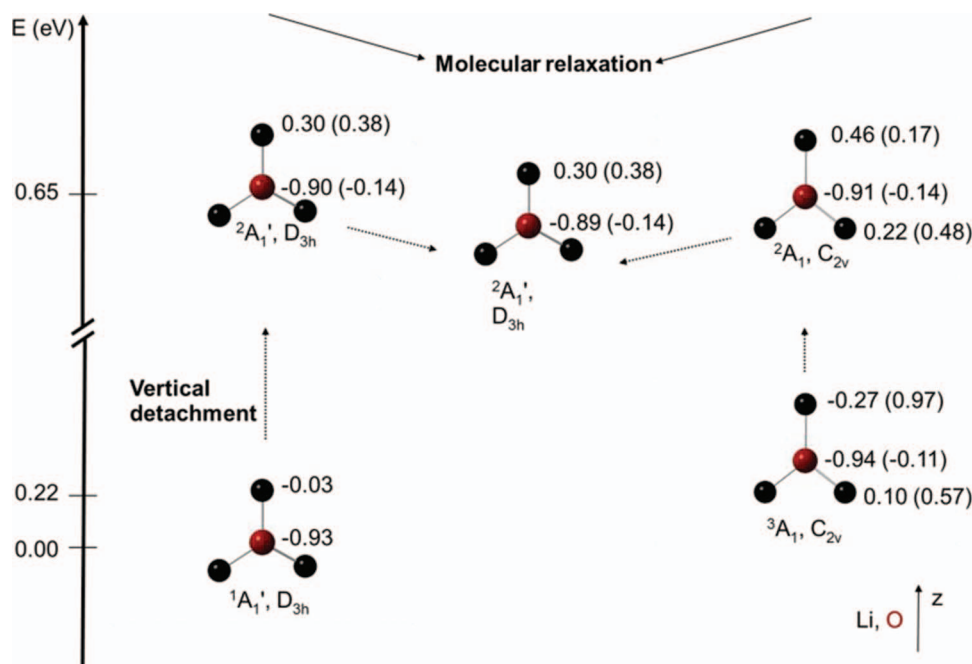


FIG. 4. Mulliken atomic charges and spin density distributions (in parenthesis when $\neq 0$). Depicted bond length differences in the C_{2v} structures are slightly exaggerated for clarity.

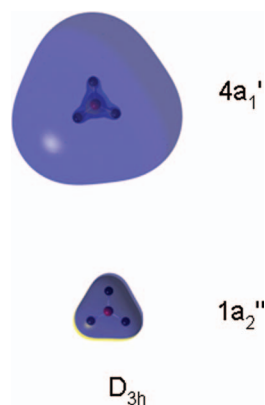


FIG. 6. Highest occupied molecular orbitals of the singlet ground state (isovalue = 0.005).

The $6a_1$ α spin-orbital is symmetric relative to the plane bisecting the lower Li-O-Li plane, which explains the sharing of one electron's spin by the two lower Li atoms. The other unpaired electron occupies the $7a_1$ α spin-orbitals, that is, localized chiefly on the upper Li atom. After electron detachment (Fig. 4, top right), it is this electron that is removed, thus the spin density on this specific Li is drastically reduced with relatively small changes in the atomic spins of the other two Li atoms. Now when the doublet molecular geometry is allowed to relax, from C_{2v} (top right) to D_{3h} (center), it will induce an electronic flux to the Li atom on the z axis from the other two, in order for the HOMO to regain D_{3h} symmetry. This is also illustrated by the decrease of positive charge of the top Li and increase of its spin density. This phenomenon marks the main difference between the effects of geometrical relaxations of the doublet states in Fig. 4.

The absolute values of the charge and density distributions can vary according to the method of analysis, e.g., the natural population analysis³⁹ or atoms in molecules⁴⁰ schemes. This should be true in our case,⁸ but here we are more interested in the charge distribution *changes* accompanying transitions rather than the absolute values. Thus, we expect the above-presented analysis to be qualitatively valid for any method. Nevertheless, it must be indicated that our Mulliken analysis supports a O^-Li_3^+ picture following Pople's description.⁹

Electron propagator theory calculations

BD-T1 gives VEDE values of 0.67 eV for the first electron detachment from the singlet with a PS of 0.82 for basis sets 1, 4, and 6. Pople basis sets with two diffuse functions (i.e., 2, 5, and 8) give the same results for the first VEDE. Basis set #10 gives similarly 0.67 eV and 0.83 for the VEDE and PS, respectively. The BD-T1 value coincides with the adiabatic result calculated at the CCSD(T) level.

The HOMO-2 and HOMO-3 are degenerate. These correspond to the p_x and p_y orbitals of the oxygen atom while the HOMO-1 is the non-bonding p_z of the oxygen. Table II results indicate that the second electron detachment from the singlet occurs at energies higher than 3.5 eV, the upper (or right hand) limit of the experimental spectrum we discuss here.

TABLE II. BD-T1 VEDEs of the $^1A_1'$ state of the anion using 6-311+G*.

Orbital	VEDE (eV)	PS
HOMO-3	5.80	0.79
HOMO-2	5.80	0.79
HOMO-1	4.93	0.85
HOMO	0.67	0.82

The P3 method was considered for the estimation of the first two VEDEs of the triplet species (Table III) since in the current implementations of BD-T1 only calculations of closed shells are available. BD-T1 calculations on the singlet show that the inner electrons are too stable for the laser energy used in the presently discussed experiments. Therefore, only singly occupied molecular orbitals are considered here ($6a_1$ and $7a_1$ α in Fig. 5). The first VEDE is very close to the first VEDE of the singlet even though the latter involves a completely different molecular orbital. The second VEDE, however, appears at about 1.2 eV and seems to be responsible for the second peak we see in the experimental spectrum. It involves an orbital that resembles the HOMO in the singlet state. This stabilization can be explained chiefly by the higher number of exchange interactions involving only the open-shell (spin up or spin down) electrons in the triplet electronic state. This number is higher for the majority spin in open-shell systems.

Table IV shows IPs (ionization potentials) of the ground and excited states of the neutral species as calculated at the D_{3h} and C_{2v} geometries of the anion. Columns 4 and 8 in Table IV indicate the hydrogen-like classification of the molecular orbitals. When higher excited states are considered, electrons occupy more diffuse Rydberg orbitals and the potential of the molecular frame resembles more a positively charged entity, as in the hydrogen atom case. They resemble very closely the Dyson orbitals and play a key role in the interpretation of the intensities and locations of the observed peaks. When the molecular orbital is spread over the molecular frame, in other words when they are engaged in bonding or antibonding interactions, one expects smaller intensities of the corresponding peak and a shift in the ionization energy since geometry changes are then expected to occur after the electron removal. This qualitative interpretation follows from the Frank-Condon factors dependence on the vibrational overlap between nuclear coordinates of the initial and final states. When the orbital involved in the transition has a non-bonding character, small changes in the molecular geometries are expected after a transition and, thus, higher overlap and larger Frank-Condon factors.

TABLE III. P3 results of the VEDEs of the triplet state of Li_3O^- . More detailed data on the influence of the basis set size on the calculated properties are given in the supplementary material (Ref. 35).

	Orbital	VEDE (eV)	PS
3A_1	HOMO-1	1.19	0.96
	HOMO	0.51	0.97

TABLE IV. Ionization potentials and symmetries of the excited neutral states of the Li_3O calculated with basis set #8 at the BD-T1 level of theory.

D_{3h}	IP	PS	H-like	C_{2v}	IP	PS	H-like
$4a_1'$	3.45	0.99	$3s$	$6a_1$	3.53	0.99	$3s$
$3e'$	2.78	0.99	$3p_y$	$7a_1$	2.83	0.99	$3p_y$
$3e'$	2.78	0.99	$3p_x$	$3b_2$	2.73	0.99	$3p_x$
$2a_2''$	2.01	0.99	$3p_z$	$2b_1$	2.03	0.99	$3p_z$
$4e'$	1.75	0.99	$3d_{(x^2-y^2)}$	$8a_1$	1.81	0.99	$3d_{(x^2-y^2)}$
$4e'$	1.75	0.99	$3d_{xy}$	$4b_2$	1.70	0.99	$3d_{xy}$
$1e''$	1.49	0.99	$3d_{xz}$	$3b_1$	1.52	0.99	$3d_{yz}$
$1e''$	1.49	0.99	$3d_{yz}$	$9a_1$	1.49	0.99	$4s$
$5a_1'$	1.47	0.99	$4s$	$1a_2$	1.45	0.99	$3d_{xz}$
$6a_1'$	1.34	0.99	$3d_{z^2}$	$10a_1$	1.34	0.99	$3d_{z^2}$
$5e'$	1.24	0.99	$4p_y$	$11a_1$	1.26	0.99	$4p_y$
$5e'$	1.24	0.99	$4p_x$	$5b_2$	1.23	0.99	$4p_x$
$3a_2''$	1.05	0.99	$4p_z$	$4b_1$	1.06	0.99	$4p_z$
$1a_2'$	0.93	0.99	$4f_{y(3x^2-y^2)}$	$6b_2$	0.93	0.99	$4f_{y(3x^2-y^2)}$
$6e'$	0.91	0.99	$4d_{(x^2-y^2)}$	$12a_1$	0.93	0.99	$4d_{(x^2-y^2)}$
$6e'$	0.91	0.99	$4d_{xy}$	$7b_2$	0.89	0.99	$4d_{xy}$
$7a_1'$	0.83	0.99	$5s$	$13a_1$	0.83	0.99	$5s$
$2e''$	0.81	0.99	$4d_{xz}$	$5b_1$	0.83	0.99	$4d_{xz}$

The HOMO of the neutral species appears to be responsible for the far right peak in the Li_3O spectrum.¹⁵ The relatively high intensity of this peak should come from its correspondence to a completely symmetric s -like orbital, and that minor geometry changes are expected after such ionization. The HOMO+1 and the HOMO+2 ($3e'$) are responsible for the peak centered at about 3.0 eV. These two polarized molecular orbitals are expected to distort slightly the geometry of the neutral species, when involved in the transition, and hence they are shifted and possess lower intensities when ionized. The observed intensive peak, at about 1.95 eV, can be attributed to the $2a_2''$, orbital that is of $3p_z$ nature, centered on the oxygen atom. The in-plane degenerate d -like MOs, HOMO+4, and HOMO+5 ($4e'$), give rise to the highest peak in the spectrum centered at about 1.75 eV. These MOs have non-bonding shapes which together with their degeneracy could explain the high intensity of the associated peak. The width of this peak may find origins in the C_{2v} geometry of the triplet together with the expected Jahn-Teller effects in the excited doublet of the D_{3h} structure.

The interpretation of the flat peak about 2.25 eVs, in the experimental spectrum, led us to the consideration of the shake-up states (Table V) corresponding to the simultaneous promotion of the molecule to an excited neutral state together with an electron detachment. This peak can be attributed to a shake-up from the ground anionic singlet state to the $4E'$ excited neutral state (2.37 eV). One can still speculate about the presence of the triplet species of the anion because the large peak centered about 1.1 eV could be the result of the photoionization of higher neutral states (HOMO+11, 12...), shake-up (to the $3E'$ state) or the photodetachment from the HOMO-1 of the triplet. It could also be the result of the convolution of these three transitions.

Our computational results are supported by the resonance enhanced two-photon ionization spectroscopy experimental spectrum reported between 0.7 and 2.75 eV.⁵ Figure 2(a) of

TABLE V. Shake-up transition energies.

Final state	Shake-up energy (eV)
$3e'$	1.34
$3e'$	1.34
$2a_2''$	2.12
$4e'$	2.37
$4e'$	2.37

Ref. 5 displays four broad absorption bands of the neutral doublet named A, B, C, and D and centered around 0.8, 1.7, 1.9, and 2.2 eV, respectively. We will also discuss here a small peak located next to B with lower intensity and we will call it here B'. In the following discussion the excitation energies between the ground and excited neutrals will be simply considered as the energy differences between the excited doublets and the ${}^2A_1'$ state calculated with the BD-T1 method. The high intensity A peak is the signature of the excitation to the first excited doubly degenerate $3E'$ states. The B peak comes from the $4E' \leftarrow {}^2A_1'$ excitation while the B' peak can be attributed to the ${}^2A_2'' \leftarrow {}^2A_1'$ excitation. The lower intensity of this peak finds its origins in the non-degeneracy of the excited state. The C peak is the result of the excitation to the $1E'' \leftarrow {}^2A_1'$ state. This peak, has a similar intensity with the A and B bands. D is the broadest of all peaks with a lower intensity, it should result from the excitation to all remaining excited states that are displayed in Fig. 7. At this energy level, the

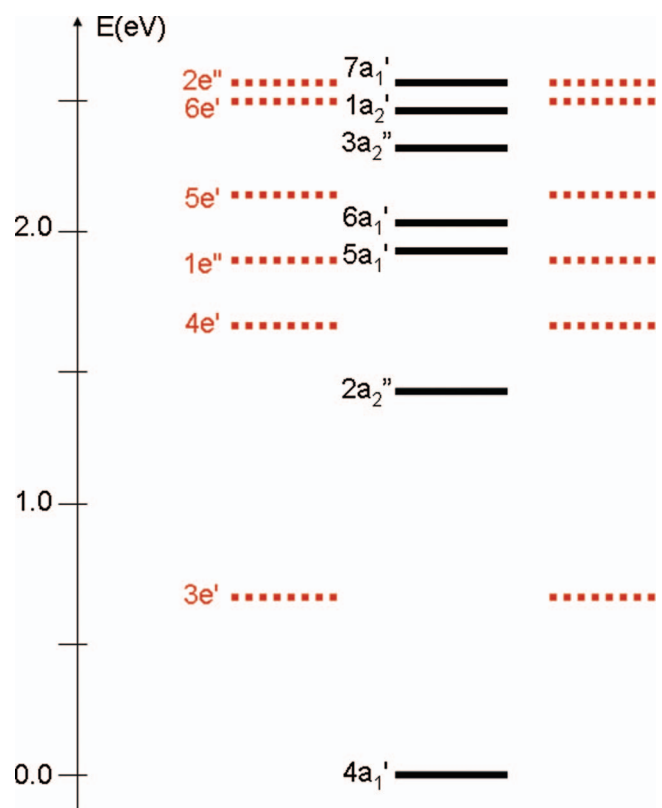


FIG. 7. Ground and excited doublet states as calculated from the BD-T1 method and basis set #8.

gaps between excited states become narrower. This explains the breadth of the experimental peak.

It is worth mentioning that numerical results on the neutral doublet ionization potentials are readily converged at the Hartree-Fock (HF) level. HF, OVGF, and P3 results for this species are very similar to those of BD-T1 displayed here. This must follow from the accuracy of the approximation we adopted of calculating the IPs of the excited neutral as the electron affinities of the cation. Also, the correlation effects are expected to be less important for the excited doublets since single electrons occupy molecular orbitals in these states. Consequently, no same-orbital correlation effects should be present. In addition, the overcounting of occupied orbitals that can be “seen” by virtuals is removed by considering the $(N-1)$ -electron system, i.e., the cation in this case.

Molecular breathing

Numerical estimation of the normal mode vibrational frequencies with the harmonic approximation using quantum chemistry methods provides, in addition to the infrared spectrum, the attribution of normal modes to specific frequencies. For example, in our case we have several electronic ground states possessing different structures; one would then be interested in following the variation of the frequencies as the structural parameters change (see supplementary material Ref. 35). At first glance, some shifts in the frequencies are expected when going from a state to another but the hierarchy of the normal modes should not change. If that were the case, we would have to attribute a b_1 irreducible representation to the lowest normal mode of the triplet in Fig. 8, for a_2'' in the D_{3h}

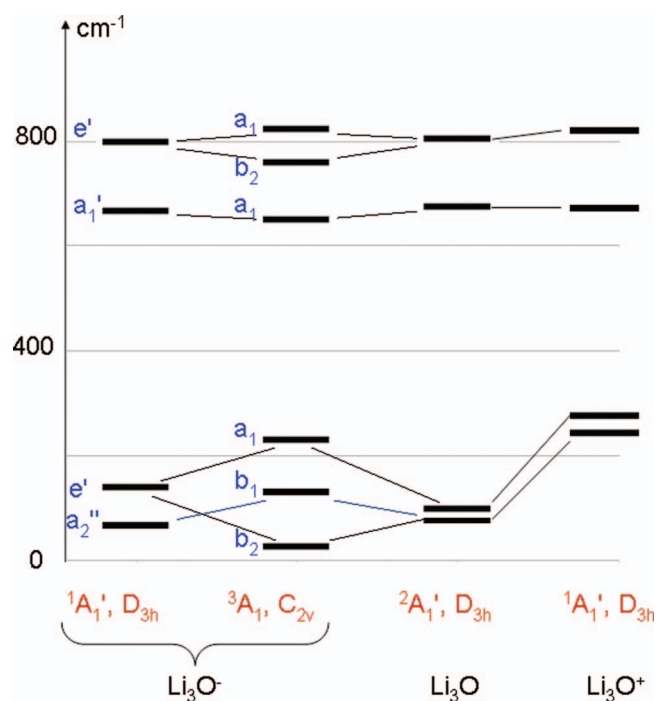


FIG. 8. Normal-mode vibrational frequencies calculated at the 6-311+G*/CCSD(T) level of theory. See Fig.1 for the associated displacement vectors. Numerical values are tabulated in the supplementary material (Ref. 35).

group leads to a b_1 irreducible representation in the C_{2v} group (the shape of the normal mode of each irreducible representation is given in Fig. 1). However, the computational analysis does not agree with this assumption. The order of the lowest b_1 and b_2 vibrations in the triplet is inverted relative to the singlet and the doublet states. Without the explicit calculation of the normal modes, using quantum chemistry techniques, this information would have been very difficult to access.

In general, the bending modes are more influenced by the change in the charge numbers than the stretching modes. The scissoring mode in the singlet state (e') vibrates more easily in the triplet state structure than in the singlet (Fig. 8). In fact, the HOMO of the anion singlet (illustrated in Fig. 6) exhibits constructive interference on the ring linking the three Li atoms. This continuity leads to the stabilization of the MO. This can be seen to some extent as strengthening the restoring force among Li atoms on the ring, leading to a more difficult displacement of the Li atoms towards C_{2v} symmetry. Thus, the change in the symmetry of this MO from $4a_1'$ to $6a_1$ (Figs. 5 and 6) leads to a softer scissoring mode. The scissoring and rocking modes (b_1 and a_1 , upper right side of Fig. 1) bend at lower frequencies in the neutral 2A_1 state. This can be attributed to the lowering of the occupation number of the HOMO (MO $4a_1'$) that weakens the restoring force discussed above.

We notice no important changes of the ZPEs associated with the structural changes. The lowering of the vibrational frequencies of some normal modes in the triplet state is compensated by the increase of other frequencies. The doublet state possesses the lowest ZPE. This can be understood mainly from the lower parts of the infrared spectra since the doublets are the lowest of all electronic states as illustrated in Fig. 8.

The influence of the vibrational motions on the electronic spectra of the hyperlithiated system was previously studied in the literature and was believed to have important effects.^{5,10} We have undertaken similar studies by scanning the electronic state levels along the normal-mode pathways. In particular, we were interested in checking the effects of the geometry changes at the far-side turning points of the anion on the excited states of the neutral species. No thermal population of the higher vibrational states was considered since the experimental temperature is believed to be too low for any of these effects to be observed. Table VI summarizes the results.

No significant changes are observed between vibrational frequencies of the D_{3h} anionic and neutral species, for bond lengths remain practically unchanged. We do not find any important influence of the vibrational motions on the IPs. Table VI shows that these changes are smaller than 0.05 eV, a negligible amount that confirms the well-known flatness of the potential energy surfaces of hyperlithiated molecules. This result does not contradict the findings of Neukermans *et al.* because here we consider the vibrational modes as the eigenvectors of the Hessian matrix and do not reduce them to one-dimensional angles and dihedrals as was done in Ref. 5. If we take the out-of-plane vibration mode as an example, we find that our displacements are different because the displacement vectors are perpendicular to the Li_3 plane while Neukermans *et al.* simulated this vibration by taking the

TABLE VI. Relative changes in the ionization potentials (eV) of the excited neutral states of the Li_3O molecule at the far-side turning point geometries of the anionic species.

MO #	Normal mode #					
	1	2	3	4	5	6
HOMO	-0.03	-0.02	-0.03	0.03	0.00	0.00
HOMO+1	-0.01	-0.05	-0.04	0.01	-0.02	-0.02
HOMO+2	-0.01	0.05	0.04	0.01	0.02	0.02
HOMO+3	-0.01	-0.01	-0.01	0.02	-0.01	0.00
HOMO+4	-0.01	-0.04	-0.03	-0.01	-0.02	-0.02
HOMO+5	-0.01	0.03	0.03	-0.01	0.02	0.02
HOMO+6	0.01	-0.02	-0.02	0.00	-0.02	-0.02
HOMO+7	0.00	0.01	0.01	0.00	0.02	0.02
HOMO+8	-0.02	0.00	0.00	0.01	-0.01	0.00
HOMO+9	0.01	0.00	0.00	0.01	0.00	0.00
HOMO+10	-0.01	-0.02	-0.01	0.01	0.00	0.00
HOMO+11	-0.01	0.02	0.01	0.01	0.00	0.00
HOMO+12	0.00	0.00	0.00	0.01	0.00	0.00
HOMO+13	0.00	0.00	0.00	-0.01	0.00	0.00
HOMO+14	0.00	-0.01	-0.01	0.00	0.00	0.00
HOMO+15	0.00	0.01	0.01	0.00	0.01	0.01

displacement vectors as tangential to the sphere centered on the oxygen, leaving the Li–O bond distance intact. While intuitively this assumption is correct, our numerical calculations at the CCSD(T) level suggest (see Fig. 1) that a small stretching is mixed with the bending assumed in Ref. 5. Our procedure is indeed incomplete since thermal populations of the lowest vibrational states ($n = 1, 2, \dots$) are not taken into account at least for the first three normal modes.

SUMMARY AND CONCLUSIONS

This paper deals with the quantum chemical interpretation of the photoelectron spectra reported recently for the hyperlithiated Li_3O^- and Li_3O species at a relatively high energy range of up to 3.5 eV.¹⁵ One of the major findings of this paper concerns the nature of the observed transitions in the experimental photoelectron spectra. The observed spectrum displays a superposition of VEDEs from anionic and neutral species.

The singlet (D_{3h} , $^1A_1'$) as well as the triplet (C_{2v} , 3A_1) anions coexist in the experimental sample. The presence of the triplet together with the singlet ground state is established by the second peak in the experimental spectrum that is centered around 1.1 eV. The numerous peaks between 1.5 and 3.5 eV cannot be attributed to lower molecular orbitals (electronic states) of the anion, singlet or triplet. Instead, they are evidence of the presence of neutral species. The sequence of events may be explained as follows. The first photon de-ionizes the anion to ground and excited neutral states of the neutral. A second photon ionizes these states to the corresponding cation. Our calculated ionization energies of the ground and excited neutral states explain most of the peaks observed between 1.5 and 3.5 eV as well as all of the features observed in previous resonance enhanced two-photon ionization spectroscopy experiments performed on the neutral doublet.⁵ We inspected the stability

of nuclear distributions other than those with a central oxygen surrounded by three lithium atoms, but every other stable nuclear distribution lies over 1.5 eV higher than the global ground state. These structures are very unlikely to be observed experimentally under regular conditions. At 0 K, no major shift in transition energies following nuclear motion along normal mode vibrations could be found. The biggest energy change, after molecular breathing, was smaller than 0.05 eV, which is negligible given the order of magnitude of the energies we are considering here.

The present work indicates that experimental and theoretical investigations of other hyperalkali systems could be as rich in complexity as those of hyperlithiated compounds. Higher laser energies and more precise experiments coupled to propagator calculations may lead to significant insights and in some cases, as shown in the present paper, corrections to old results. Therefore, we are undertaking further investigations on hypersodiated and hyperpotassiated systems.

ACKNOWLEDGMENTS

This work was supported by the National Science Foundation (NSF) through grant (Grant No. CHE-0809199) to Auburn University. The authors thank O. Dolgounitcheva and V. G. Zakrzewski for technical assistance and valuable discussions.

- ¹A. C. Reber, S. N. Khanna, and A. W. Castleman, *J. Am. Chem. Soc.* **129**, 10189 (2007).
- ²G. L. Gutsev and A. I. Boldyrev, *Chem. Phys. Lett.* **92**, 262 (1982).
- ³M. Gutowski and J. Simons, *J. Phys. Chem.* **98**, 8326 (1994).
- ⁴K. Yokoyama, H. Tanaka, and H. Kudo, *J. Phys. Chem. A* **105**, 4312 (2001).
- ⁵S. Neukermans, E. Janssens, H. Tanaka, R. E. Silverans, P. Lievens, K. Yokoyama, and H. Kudo, *J. Chem. Phys.* **119**, 7206 (2003).
- ⁶H. Kudo, C. H. Wu, and H. R. Ihle, *J. Nucl. Mat.* **78**, 380 (1978); H. Kudo, *Nature (London)* **355**, 432 (1992).
- ⁷C. H. Wu, H. Kudo, and H. R. Ihle, *J. Chem. Phys.* **70**, 1815 (1979).
- ⁸P. Lievens, P. Thoen, S. Bouckaert, W. Bouwen, F. Vanhoutte, H. Weidele, R. E. Silverans, A. Navarro-Vázquez, and P. von Ragué Schleyer, *J. Chem. Phys.* **110**, 10316 (1999).
- ⁹P. V. R. Schleyer, E. U. Wuerthwein, and J. A. Pople, *J. Am. Chem. Soc.* **104**, 5839 (1982).
- ¹⁰H. Kudo, *J. Nucl. Radiochem. Sci.* **2**, R13 (2001).
- ¹¹E. Rehm, A. I. Boldyrev, and P. V. R. Schleyer, *Inorg. Chem.* **31**, 4834 (1992).
- ¹²V. Bonačić-Koutecký, J. Pittner, R. Pou-Amerigo, and M. Hartmann, *Z. fuer Physik D* **40**, 445 (1997).
- ¹³R. J. Bartlett, *J. Phys. Chem.* **93**, 1697 (1989).
- ¹⁴K. Raghavachari, G. W. Trucks, J. A. Pople, and M. Head-Gordon, *Chem. Phys. Lett.* **157**, 479 (1989).
- ¹⁵D. Wang, J. D. Graham, A. M. Buytendyk, and K. H. Bowen, Jr., *J. Chem. Phys.* **135**, 164308 (2011).
- ¹⁶W. von Niessen, J. Schirmer, and L. S. Cederbaum, *Comput. Phys. Rep.* **1**, 57 (1984).
- ¹⁷J. V. Ortiz, *J. Chem. Phys.* **104**, 7599 (1996).
- ¹⁸R. A. Chiles and C. E. Dykstra, *J. Chem. Phys.* **74**, 4544 (1981).
- ¹⁹N. C. Handy, J. A. Pople, M. Head-Gordon, K. Raghavachari, and G. W. Trucks, *Chem. Phys. Lett.* **164**, 185 (1989).
- ²⁰J. V. Ortiz, *Int. J. Quantum Chem.* **75**, 615 (1999).
- ²¹J. V. Ortiz, *Chem. Phys. Lett.* **296**, 494 (1998).
- ²²J. V. Ortiz, *Adv. Quantum Chem.* **35**, 33 (1999).
- ²³I. G. Kaplan, B. Barbiellini, and A. Bansil, *Phys. Rev. B* **68**, 235104 (2003).
- ²⁴E. Weigold and I. E. McCarthy, *Electron Momentum Spectroscopy* (Kluwer Academic/Plenum Publishers, New York, 1999).
- ²⁵M. S. Deleuze and S. Knippenberg, *J. Chem. Phys.* **125**, 104309 (2006).

- ²⁶J. Itatani, J. Levesque, D. Zeidler, H. Niikura, H. Pepin, J. C. Kieffer, P. B. Corkum, and D. M. Villeneuve, *Nature (London)* **432**, 867 (2004).
- ²⁷S. Patchkovskii, Z. Zhao, T. Brabec, and D. M. Villeneuve, *Phys. Rev. Lett.* **97**, 123003 (2006).
- ²⁸M. Yamazaki, T. Horio, N. Kishimoto, and K. Ohno, *Phys. Rev. A* **75**, 032721 (2007).
- ²⁹R. Flores-Moreno, J. Melin, O. Dolgounitcheva, V. G. Zakrzewski, and J. V. Ortiz, *Int. J. Quantum Chem.* **110**, 706 (2010).
- ³⁰J. W. Rabalais, *Principles of Ultraviolet Photoelectron Spectroscopy* (John Wiley and Sons, New York, 1977).
- ³¹M. J. Frisch, G. W. Trucks, H. B. Schlegel *et al.*, GAUSSIAN 03, Gaussian, Inc., Wallingford, CT, 2003.
- ³²R. Krishnan, J. S. Binkley, R. Seeger, and J. A. Pople, *J. Chem. Phys.* **72**, 650 (1980).
- ³³M. J. Frisch, J. A. Pople, and J. S. Binkley, *J. Chem. Phys.* **80**, 3265 (1984).
- ³⁴J. Lindenberg and Y. Öhrn, *Propagators in Quantum Chemistry*, 2nd ed. (John Wiley and Sons, Hoboken, New Jersey, 2004).
- ³⁵See supplementary material at <http://dx.doi.org/10.1063/1.3636082> for the basis set effects and normal mode vibrational frequencies.
- ³⁶K. A. Peterson, D. E. Woon, and T. H. Dunning, *J. Chem. Phys.* **100**, 7410 (1994).
- ³⁷G. D. Purvis and R. J. Bartlett, *J. Chem. Phys.* **76**, 1910 (1982).
- ³⁸R. O. Jones, A. I. Lichtenstein, and J. Hutter, *J. Chem. Phys.* **106**, 4566 (1997).
- ³⁹A. E. Reed, L. A. Curtiss, and F. Weinhold, *Chem. Rev.* **88**, 899 (1988).
- ⁴⁰R. F. W. Bader, *Atoms in Molecules: A Quantum Theory* (Oxford University Press, New York, USA, 1994).